Mid-infrared frequency domain optical parametric amplifier

Gilles Dalla-Barba, Gaëtan Jargot, Philippe Lassonde, Szabolcs Tóth, Elissa Haddad, Fabio Boschini, Jean-Christophe Delagnes, Adrien Leblanc, Heide Ibrahim, Eric Cormier, et al.

Research Article | Vol. 31, No. 9 / 24 Apr 2023 / Optics Express 14954
Optics EXPRESS

Mid-infrared frequency domain optical parametric amplifier

GILLES DALLA-BARBA,[1,2] GAËTAN JARGOT,[1] PHILIPPE LASSONDE,[1] SZABOLCS TÓTH,[3] ELISSA HADDAD,[1] FABIO BOSCHINI,[1] JEAN-CHRISTOPHE DELAGNES,[4] ADRIEN LEBLANC,[5] HEIDE IBRAHIM,[1] ERIC CORMIER,[2,6] AND FRANÇOIS LÉGARÉ[1,*]

[1]*Advanced Laser Light Source (ALLS) at the Institut National de la Recherche Scientifique, Centre Énergie Matériaux et Télécommunications, 1650 Boulevard Lionel-Boulet, Varennes, Québec J3X 1S2, Canada*
[2]*Laboratoire Photonique Numérique et Nanosciences (LP2N), UMR 5298, CNRS-IOGS-Université Bordeaux, 33400 Talence, France*
[3]*ELI-ALPS Research Institute, Dugonics tér 13, 6720 Szeged, Hungary*
[4]*Centre National de la Recherche Scientifique, Centre Lasers Intenses et Applications, 351, Cours de la Libération, Talence, France*
[5]*Laboratoire d'Optique Appliquée, Ecole Polytechnique, ENSTA, CNRS, Université Paris Saclay, Palaiseau, France*
[6]*Institut Universitaire de France (IUF), 1 rue Descartes, 75231 Paris, France*
[*]*legare@emt.inrs.ca*

Abstract: We report on an optical architecture delivering sub-120 femtosecond laser pulses of 20 µJ tunable from 5.5 µm to 13 µm in the mid-infrared range (mid-IR). The system is based on a dual-band frequency domain optical parametric amplifier (FOPA) optically pumped by a Ti:Sapphire laser and amplifying 2 synchronized femtosecond pulses each with a widely tunable wavelength around 1.6 and 1.9 µm respectively. These amplified pulses are then combined in a GaSe crystal to produce the mid-IR few-cycle pulses by means of difference frequency generation (DFG). The architecture provides a passively stabilized carrier-envelope phase (CEP) whose fluctuations has been characterized to 370 mrad RMS.

1. Introduction

During the last decades, generation of few-cycle pulses in the mid-infrared spectral range (mid-IR) has experienced a growing interest for numerous applications both in strong-field physics [1–8] and molecular spectroscopy [9–12]. The generation of XUV photons by means of high-harmonic generation (HHG) is intrinsically connected to the energy of electrons as they get accelerated by the driving field and directly linked to their ponderomotive energy. This connection is well established for HHG in gaseous media but still under debate for HHG in solids. Due to the quadratic scaling of the electron ponderomotive energy with the driving laser wavelength, mid-IR pulses allow to significantly increase the harmonic cutoff compared to shorter wavelength; however at a cost of efficiency [13]. While HHG in gaseous media has been studied for decades now, its counterpart in transparent solid media is rather new [2]. To drive HHG from solid targets, in particular from low bandgap materials such as semiconductors and quantum materials [14–16], there is a need for long wavelength (usually above 1.5 µm) and energetic (several µJ) laser pulses. Such sources will allow to maintain the interaction in the tunneling regime where the system can withstand significantly stronger intensities leading to highly non-linear processes.

Up to now, realizations of mid-IR few-cycle pulses above the microjoule are still scarce, as depicted in Fig. 1 for wavelengths between 4 µm and 14 µm [17–29]. These realizations are designed for either a fixed wavelength, or a limited tunable range in the mid-IR spectral range.

#487813 https://doi.org/10.1364/OE.487813
Journal © 2023 Received 16 Feb 2023; revised 16 Mar 2023; accepted 17 Mar 2023; published 20 Apr 2023

Optics EXPRESS

A noticeable work reporting a tunable mid-IR source is the recent work of Budriünas in 2022 [17] where µJ level pulses are produced with wavelengths extending from 4 to 11 µm. In this context, we present here an alternative optical architecture to generate sub-120 fs pulses duration with around 20 µJ of energy at a central wavelength tunable from 5.5 to 13 µm, with a passively stabilized carrier-envelope phase (CEP).

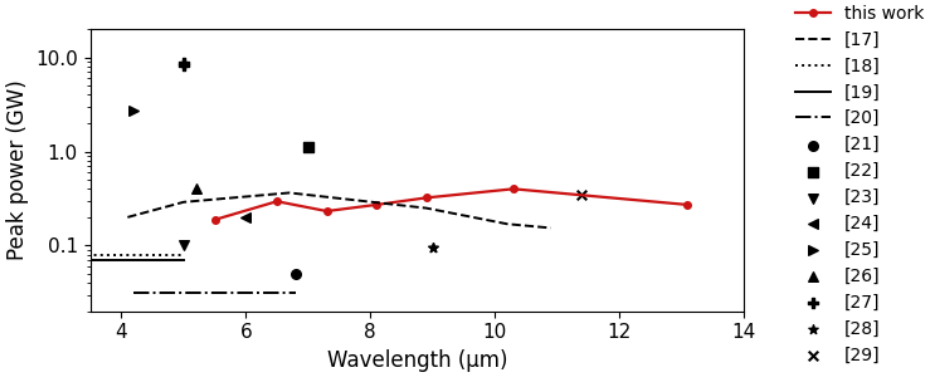

Fig. 1. State of the art microjoule few-cycle mid-IR sources between 4 µm and 14 µm. Wavelength-tunable sources are represented in solid lines and fixed wavelengths with symbols. The grey dashed line refers to the data labelled "DFG no window" in Fig. 7 of Ref. [26].

This architecture is based on the frequency domain optical parametric amplifier (FOPA) [30], which provides the possibility to amplify frequency components in a slice-by-slice manner leading to high gain [31] and high-power [32] amplification records. In addition to pure amplification operations, the field of frequency domain nonlinear optics was established for advanced manipulations [33,34].

2. Experimental setup

In this paper, the mid-IR source is based on the frequency conversion of a 100 Hz repetition rate Ti:Sapphire laser delivering 45 fs pulses centered at 790 nm (available at the Advanced Laser Light Source user facility). Figure 2 depicts a general overview of the optical setup which is an extension of an earlier setup reported in [34]. First, the output of the Ti:Sapphire laser is divided into two optical arms of 5 mJ and 30 mJ (±1.3% RMS), which are compressed to a pulse duration of respectively 45 fs and 1.15 ps. In one arm (bottom of Fig. 2), the 5 mJ pulses are converted from 790 nm to 1.75 µm using a commercial optical parametric amplifier (OPA, TOPAS, Light Conversion) with an efficiency of 16%. The spectra of the resulting 0.8 mJ (±3% RMS) pulses are then broadened to a bandwidth of about 400 nm by propagating in a 1.7 meter long hollow-core fiber (HCF) of 1 mm diameter, filled with 1.65 bar of krypton (Few-cycle Inc.). After the fiber, the beam is expanded to reach a diameter of 7 mm with a two-lens telescope (f = -500/+1000 mm) to serve as a seed for FOPA. In the other arm (top of Fig. 2), the 30 mJ pulses are split in two equal parts of 15 mJ in order to pump non collinearly two spectral bands of the FOPA. As the seed is spatially dispersed in this plane (see later and in Fig. 3 for details), the interaction of the beams in a 5 mm thick BBO crystals results in the parametric amplification at millijoule level of two spectral bands at 1.6 µm and 1.9 µm respectively. Finally (bottom right of Fig. 2), the bicolor beam carrying pulses of 100 fs propagates through a 0.75 mm thick, z-cut uncoated GaSe crystal with 15 mm diameter (Altos Photonics) to generate mid-IR pulses by difference frequency generation (DFG).

The innovative features of this source are provided by the design of the FOPA, which is detailed in Fig. 3(a). In the Fourier plane (F-plane), located at the center of the optical system,

Optics EXPRESS

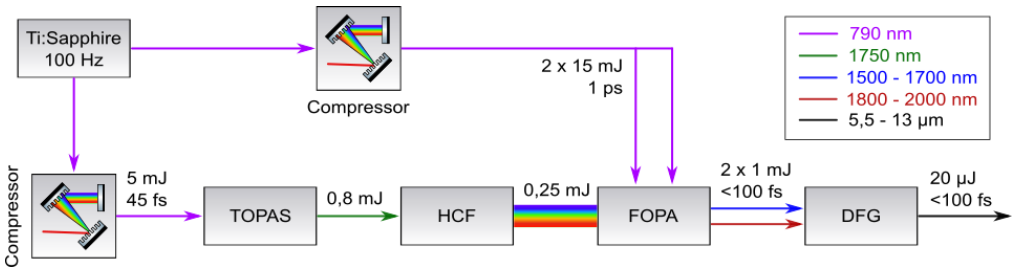

Fig. 2. Optical architecture of the mid-IR source where TOPAS is an industrial OPA, HCF is a stretched hollow-core fiber, FOPA a Frequency domain Optical Parametric Amplifier and DFG a difference frequency generation stage.

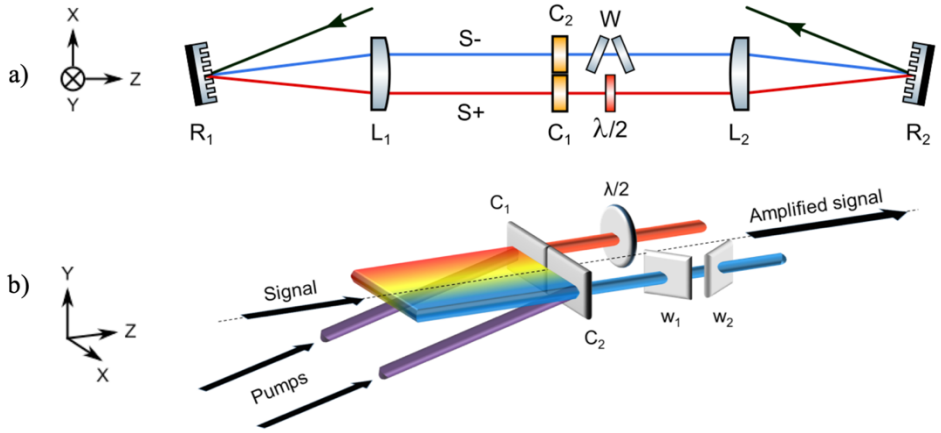

Fig. 3. (a) Dual-band FOPA design with R1/R2 gratings of 75 lines/mm period, L1/L2 cylindric lenses of +750 mm focal length, C1/C2 BBO crystals of 5 mm thickness, W1/W2 silica windows of 0.5 mm thickness, λ/2 a half-waveplate and S+/- being the selected reddest/bluest part of the seed spectrum. (b) 3D view of the Fourier plane at the center of the FOPA.

the broadband seed is spatially spread and subsequently confined over 4 cm in one transverse direction (X axis on Fig. 3) by a pair of diffraction grating (R1) and cylindric lens (L1) of respectively 75 lines/mm period and +750 mm focal length in a 2-f configuration. In the other direction (Y), the beam is only experiencing free-space propagation. Due to the wavelength separation in X axis in the F-plane, the pulse duration in this location is estimated to about one picosecond and the pump pulse duration is adjusted accordingly to optimize the temporal overlap. In the spatial domain, both pump beams are collimated to 8 mm diameter, so the spatial overlap between the diffracted seed and the pumps is concentrated to two spatial bands, as depicted in Fig. 3 (b). Two BBO crystals of (C1 and C2) are inserted in the F-plane at locations covering the selected wavelength to be amplified. The two spatially separated overlaps between seed and pump beams lead to the amplification of two spectral bands, labelled as S + and S- in Fig. 3(a). Right after amplification, the polarization of S + is rotated by 90° with a half-waveplate (λ/2) for difference frequency generation in the type II GaSe crystal. The delay generated by the plate on S + is compensated by a pair of 0.5 mm thick silica tilted windows on S- (W1 and W2). Finally, the amplified spectral components of the seed are recombined by a symmetrical 2-f setup (L2 and R2) while the non-converted pumps (non collinear and thus spatially separated) are dumped just before L2.

Optics EXPRESS

3. Results and discussions

At the output of the FOPA, the optical beam carries two pulses with sub-100 fs duration, both spatially and temporally overlapped. Depending on the transverse position of the two pump beams in the Fourier plane (X axis), the central wavelength of each amplified pulse can be tuned all along the seed spectrum from 1.5 µm to 2.0 µm. Figure 4(a) shows the seed spectrum of the FOPA (solid black line) and a typical pair of amplified spectra (solid blue and red lines) measured after the last grating of the FOPA. The output pulse durations have been characterized using second harmonic generation frequency resolved optical gating (SHG-FROG) for different amplified bands (from 1.52 to 2.02 µm). Figures 4(b), (c) show the pulse duration associated to the blue and red amplified spectra displayed in Fig. 4(a) with respectively 83 fs and 89 fs at full width half maximum (FWHM). The temporal characterization of both beams is also given in Fig. 4(d) while the wavelength is tuned in the ranges within 1.5 - 1.7 µm for S- and within 1.8 - 2.0 µm for S + .

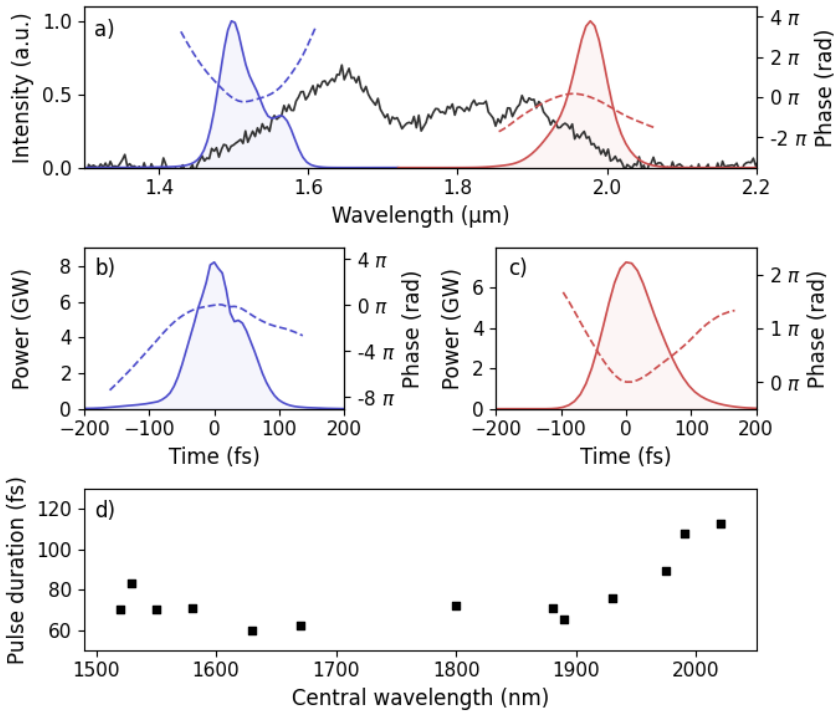

Fig. 4. (a) Seed spectrum (black), amplified spectra (solid red/blue) and spectral phase (dashed red/blue). (b-c) Temporal profile (solid) and phase (dashed) of amplified pulses S + (red) and S- (blue). (d) FWHM pulse duration vs. amplified center wavelength.

As both spatial and temporal intensity distributions of the pumps are Gaussian, the spatial beam profile of the seed is significantly modified by the gain narrowing experienced in the FOPA. It's important to distinguish the narrowing along either dispersed (X) or non-dispersed (Y) axis. On the Y axis, there is no spatio-temporal distortion so the narrowing is directly linked to the spatial gaussian distribution of the pump (the gain at the center of the beam is higher than the gain in the edges). In contrast, on the X axis the seed is affected by ultrafast wavefront rotation in the F-plane, also known as ultrafast lighthouse effect or time vs. angle [35]. In the presence of this spatio-temporal distortion, the direction of the propagation k-vector rotates over the duration of the pulse, so the angular distribution of amplified k-vectors in the F-plane is shaped by the

Optics EXPRESS

temporal gain profile. For a Gaussian pump pulse profile, this phenomenon results at the output of the FOPA in a spatial narrowing of the amplified beam along the X axis. In our setup, to preserve a non-elliptic amplified beam, the FOPA setup has been designed to equalize the gain narrowing on both dispersed and non-dispersed axis considering spatial and temporal Gaussian pump profiles. Figure 5 shows the experimental spatial profiles of a pair of two amplified beams at 1900nm (panel a) and 1700nm (panel b) separately and overlapped (panel c). The beam profiles have been measured with a silicon-based CCD camera used in the two-photon absorption regime and located five meters after the last grating of the FOPA. For each acquisition, the square root of the intensity is calculated to account for the two-photon detection and measure the intensity distribution. On Fig. 5(a), (b), the beam profiles at 1700nm and 1900nm have been isolated by masking one of the BBO crystals in the F-plane. For a pump pulse duration of 1.15 ps, which gives the maximum conversion efficiency, the dimensions of the seed beams reduce from 7 mm (no amplification) to around 4 mm (nominal amplification) without degradation of ellipticity.

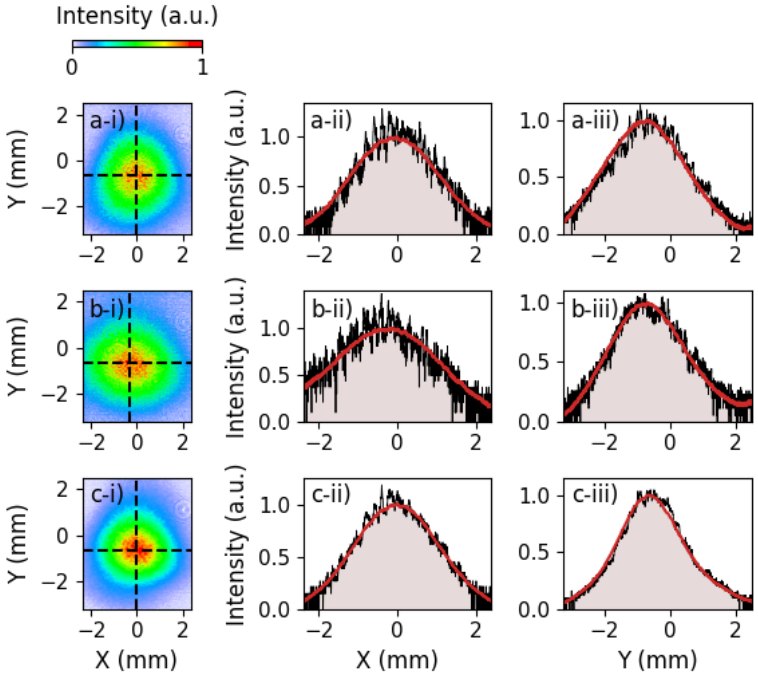

Fig. 5. (i) Amplified spatial mode measured 5 meters after the FOPA output for (a) the 1700nm beam, (b) the 1900nm beam and (c) both beams overlapped. In (ii) and (iii), the transverse intensity profile (black) at the centroid of the beam in the FOPA dispersive (X) and non-dispersive (Y) axes, and the integrated intensity (red) are shown.

At the output of the FOPA, the two amplified spectral components S- and S + are geometrically recombined into a single beam. The pulses are temporally overlapped and serve as pump (S+) and signal (S-) beams of the final DFG stage of the setup (performed in a GaSe crystal). Considering the spatial profile of Fig. 5(c), the combined pump and signal intensities reach around 100 GW/cm^2 in the DFG crystal, which is similar to multiples works of DFG in GaSe [17,36,37]. At our repetition rate of 100 Hz, the crystal is preserved from undesirable thermal effects.

This final stage consists in a collinear DFG carried out in a 0.75 mm long GaSe crystal, providing idler pulses with up to 20 microjoules of energy in the mid-IR. By selecting the respective wavelengths of the signal and the pump (adjustable between 1.5 µm and 2.0 µm in the FOPA), a tunability range extending from 5.5 µm to 13 µm has been achieved. The closer

Optics EXPRESS

the two amplified slices S- and S + are spectrally (placed together in the F-plane), the longer the resulting idler wavelength is, and vice versa. While the DFG emission cutoff at short wavelength is imposed by the limited bandwidth of the FOPA seed, longer wavelengths could in principle be generated by amplifying spectral components even closer in the FOPA. However, our architecture sets geometrical limitations in the potential to select and amplify very close spectral bands. For example, the holder of the waveplate (commercial) inserted in one arm after the BBO would clip the second arm if it were too close. Using a free standing waveplate would allow to bring the 800 nm pump beams closer together in the F-plane and so generate mid-IR pulses with wavelength in excess of 15 µm. Figure 6 shows the experimental spectra (black) obtained for several positions of the 800 nm pump beams in the F-plane of the FOPA. For each configuration, both BBO crystal angles were adjusted to achieve optimal phase-matching. After the DFG stage, both non-converted signal and pump beams are filtered out with two long-pass filters (Spectrogon LP2000 and LP3500). By analyzing the data, it appeared that the transmission of this pair of filters was not uniform above 12 µm, so the mid-IR spectra at 11 µm (Fig. 6(f)) and 13 µm (Fig. 6(g)) have been corrected for the optical response of the long-pass filters. For each experimental result presented in Fig. 6, a full simulation of the DFG process (red) in GaSe has been conducted by using a 4D numerical code, accounting for spatial and temporal dependences [38,39]. The code takes into account dispersion, diffraction, absorption, birefringence, refraction on crystal surfaces and second-order nonlinearity ($\chi^{(2)}$). The 3D input fields for the simulation can be initialized from experimentally obtained data. In the current case, the temporal shape and phase for each signal-pump pair have been retrieved with SHG-FROG. In the spatial domain, the intensity profile of Fig. 5(c) has been applied to every signal and pump beams assuming a flat spatial phase (collimated beam without wavefront distortion). By using the constructed spatiotemporal shape and the measured pulse energy values, realistic input pump and signal fields were created. In these conditions, the simulated spectra fit quite well with the experimental ones. Note here that the simulations predict a non-negligible back-conversion and an efficiency (ratio between idler energy and the sum of pump and signal pulse energy) around 2%, according to state-of-the-art in GaSe [40,41]. Experimentally, we rather obtained 1% which may be attributed to ageing of our GaSe crystal and to possible imperfections on signal and pump spatial amplitude and phase profiles. As the source is tunable, efficiency has been characterized at each mid-IR wavelength. Depending on the wavelengths amplified in the FOPA, we measured at the input of the DFG stage a pump pulse energy between 0.7 mJ and 1.0 mJ and a signal energy between 0.6 mJ and 1.1 mJ. After the DFG, the idler energy lied between 18 µJ and 26 µJ, corresponding to efficiencies between 0.9% and 1.7% over the full tunability range of the source.

For all configurations spanning the range from 5.5 µm to 13 µm, the mid-IR pulses have been fully characterized by FROSt, a phase-matching-free retrieval method based on transient absorption in low-bandgap semiconductors [42]. Here, the FROSt measurements are carried out with Silicon (Si) for pulses below 9 µm and with Germanium (Ge) above 9 µm. Although both materials are transparent over the spectral band of interest, the absorption contrast is higher with Si while the transmission of Ge extends further in the mid-IR. In both cases, the Si or Ge sample used in the FROSt is pumped with a leak from the non-absorbed signal in the DFG process. This signal, at a central wavelength of around 1.9 µm, is picked from the reflection of a long-pass filter LP2500 and then frequency doubled to around 950 nm in a BBO crystal to obtain a photon energy exceeding the bandgap of both Si and Ge while ensuring a passive synchronization with the mid-IR pulses. Fortuitously, the pump around 1.6 µm is also slightly frequency doubled at around 800 nm in the BBO crystal but can easily be removed by a pair of bandpass filters 900-1150 nm before Si (or Ge) to prevent any bias in the retrieval process. Figure 7 shows the FROSt characterization of mid-IR pulses at 8 µm with a retrieved pulse duration of 81 fs FWHM (3 optical cycles at this wavelength) and a peak power of 0.26 GW. Repeating the measurement for every pulse central wavelength, we found pulse durations between 45 fs and 117 fs (i.e. 1.3 to

Optics EXPRESS

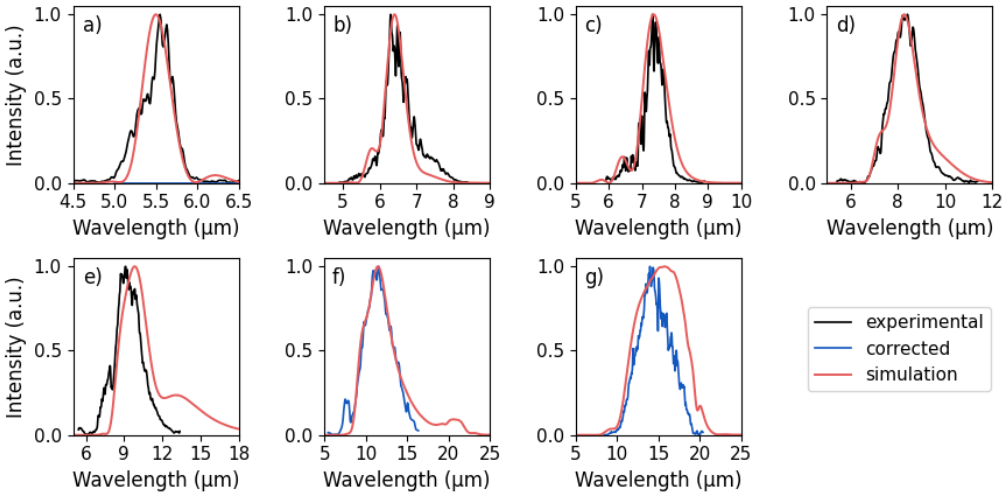

Fig. 6. Tuned experimental (black) and simulated (red) DFG spectra recorded after the GaSe crystal. For (f) and (g), measurements have been corrected by the transmission of the filters used to remove unconverted signal and pump (blue).

6.4 optical cycles) and average peak power of 0.25 GW (measured pulse energies and durations are summarized in Fig. 1). By focusing, for instance, the beam to about 100 μm diameter, such pulses can easily reach intensities above 10^{12} W/cm^2 for driving highly nonlinear processes in solids.

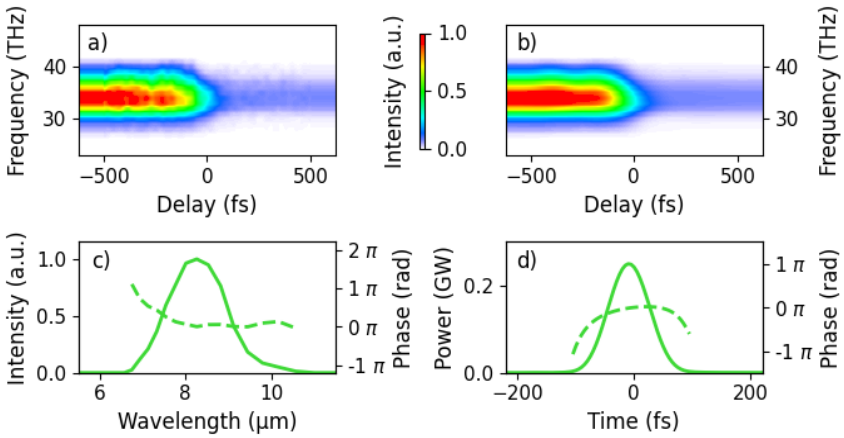

Fig. 7. FROSt characterization of the idler pulses at 8 μm. (a) Experimental trace. (b) Reconstructed trace. (c) Retrieved spectral intensity (solid) and phase (dashed). (d) Retrieved temporal intensity (solid) and phase (dashed).

Due to the fixed phase relationship between the signal and the pump involved in the DFG process, the CEP of the mid-IR pulses is passively stabilized [43]. Moreover, the actual value of the CEP can be controlled by tuning the delay between the two pulses within the FOPA by rotating one of the compensating windows in the F-plane (labelled W2 in Fig. 3). By using a characterization method based on HHG in a zinc selenide (ZnSe) crystal, CEP fluctuations have been estimated to a value of 370 mrad RMS at 9.5 μm [44] and at 6 μm (this work). A measurement at 13 μm has also be processed but the result was not reliable (see below for details).

Optics EXPRESS

Figure 8 shows the CEP characterization setup (on top) and the HHG spectra versus CEP (on bottom) obtained from mid-IR driving pulses centered at 6 µm, 10 µm and 13 µm. For each of these wavelengths, the mid-IR beam is focused in a 0.5 mm thick polycrystaline ZnSe by a 50 mm RFL (reflected focal length) off-axis parabolic mirror. The generated harmonics are focused on the input slit of a spectrometer (Ocean Optics, NIR256-2.5) by a convex lens of 25 mm focal length. At 6 µm, the HHG process is driven by nearly 5.5 optical cycles, so the features of the harmonic spectra are poorly sensitive to CEP changes. This small dependence is however sufficient to retrieve the shot-to-shot CEP value with a simple correlation function. At 10 µm, in a regime of around 2 optical cycles, the retrieval is more obvious because the HHG spectrum shifts directly with the CEP. At 13 µm, the pulse duration becomes close to the optical cycle and harmonics are only emitted at CEP values for which the field is strong enough to trigger the HHG process. In this regime, the characterization method is no longer able to retrieve the shot-to-shot CEP because the mid-IR pulse energy fluctuations are correlated with the CEP fluctuations in the resulting HHG spectra. In principle, these parameters could be decorrelated with a synchronized shot-to-shot mid-IR energy and HHG spectrum measurement associated to a calibration of HHG response versus mid-IR pulse energy (integrated and repeated along a range of CEP values). At our repetition rate of 100 Hz, the preliminary step of the method, which consists in a massively averaged scan of HHG spectrum versus CEP offset [44], took around ten minutes. This time could be fairly reduced to one minute by working at kHz repetition rate. On the other hand, the shot-to-shot retrieval calculation is fast and could suit with real-time implementation.

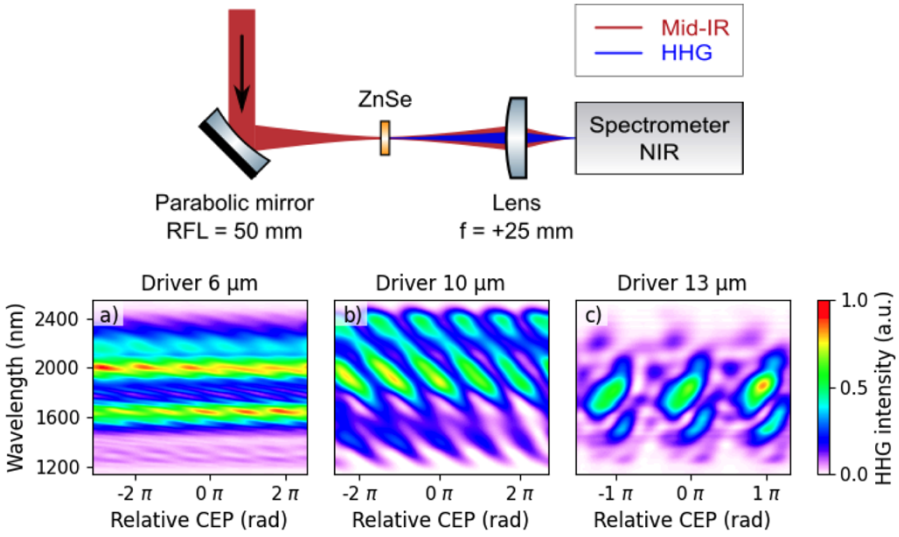

Fig. 8. Top: experimental setup of CEP fluctuation measurement. Bottom: HHG spectrum vs. CEP of a mid-IR driver centered at (a) 6 µm, (b) 10 µm and (c) 13 µm.

4. Conclusion

In this paper, we demonstrate an approach for generating widely tunable, few-cycle, CEP stable mid-IR pulses based on the combination of a dual-band FOPA and a DFG stage. With this optical architecture we have demonstrated experimentally a tunability in the mid-IR ranging from 5.5 µm up to 13 µm of high-field pulses with around 0.25 GW peak power and with very short pulse durations (close to one optical cycle at 13 µm). All over the tunability range, the pulse duration has been retrieved using FROSt, revealing the great interest of this method in this context. Thanks to an intra-band DFG architecture, the CEP of the source is self-stabilized and even

Optics EXPRESS

continuously controllable by changing the delay between pump and signal with the orientation of a window in the Fourier plane of the FOPA. CEP fluctuations have been characterized to 370 mrad RMS at 6 µm and 9.5 µm with a method base on HHG in solids. The measurement at longer wavelength, near single optical cycle duration, was not successful and will require an extension of the characterization protocol.

Through its performances and versatility, this mid-IR source brings potential solutions for studying the impact of pulse duration, wavelength and/or CEP in high-field applications such as high-harmonic generation in solids. For instance, to pursue the work exposed at the end of this manuscript, the mid-IR source could be used to fully investigate the transition between the multi-cycles and single-cycle regime when driving HHG in solids. For the future, state of the art in post-compression of high repetition rate picosecond lasers may also allow to transpose this dual-band FOPA architecture to Ytterbium or even Holmium technologies. This could be a way to increase significantly the average power or energy of the mid-IR sources, which currently imposes a strong limitation in terms of signal-to-noise ratio for many measurements associated to high-field experiments.

Funding. Natural Sciences and Engineering Research Council of Canada; European Commission (GINOP-2.3.6-15-2015-00001); Institut Universitaire de France; Fonds de recherche du Québec – Nature et technologies; PROMPT - Québec; Ministère de l'Économie, de l'Innovation et de l'Énergie - Québec; Canada Foundation for Innovation.

Acknowledgments. The authors acknowledge technical support from Antoine Laramée.

Disclosures. The authors declare no conflicts of interest.

Data availability. Data underlying the results presented in this paper are not publicly available at this time but may be obtained from the author upon reasonable request.

References

1. P. Colosimo, G. Doumy, C. I. Blaga, J. Wheeler, C. Hauri, F. Catoire, J. Tate, R. Chirla, A. M. March, G. G. Paulus, H. G. Muller, P. Agostini, and L. F. DiMauro, "Scaling strong-field interactions towards the classical limit," Nat. Phys. **4**(5), 386–389 (2008).
2. S. Ghimire, A. D. DiChiara, E. Sistrunk, P. Agostini, L. F. DiMauro, and D. A. Reis, "Observation of high-order harmonic generation in a bulk crystal," Nat. Phys. **7**(2), 138–141 (2011).
3. G. Herink, D. R. Solli, M. Gulde, and C. Ropers, "Field-driven photoemission from nanostructures quenches the quiver motion," Nature **483**(7388), 190–193 (2012).
4. T. Popmintchev, M.-C. Chen, and D. Popmintchev, *et al.*, "Bright Coherent Ultrahigh Harmonics in the keV X-ray Regime from Mid-Infrared Femtosecond Lasers," Science **336**(6086), 1287–1291 (2012).
5. O. Schubert, M. Hohenleutner, F. Langer, B. Urbanek, C. Lange, U. Huttner, D. Golde, T. Meier, M. Kira, S. W. Koch, and R. Huber, "Sub-cycle control of terahertz high-harmonic generation by dynamical Bloch oscillations," Nat. Photonics **8**(2), 119–123 (2014).
6. B. Wolter, M. G. Pullen, A.-T. Le, M. Baudisch, K. Doblhoff-Dier, A. Senftleben, M. Hemmer, C. D. Schröter, J. Ullrich, T. Pfeifer, R. Moshammer, S. Gräfe, O. Vendrell, C. D. Lin, and J. Biegert, "Ultrafast electron diffraction imaging of bond breaking in di-ionized acetylene," Science **354**(6310), 308–312 (2016).
7. J. Li, X. Ren, Y. Yin, K. Zhao, A. Chew, Y. Cheng, E. Cunningham, Y. Wang, S. Hu, Y. Wu, M. Chini, and Z. Chang, "53-attosecond X-ray pulses reach the carbon K-edge," Nat. Commun. **8**(1), 186 (2017).
8. Z. Chang, L. Fang, and V. Fedorov, *et al.*, "Intense infrared lasers for strong-field science," Adv. Opt. Photonics **14**(4), 652 (2022).
9. A. Schliesser, N. Picqué, and T. W. Hänsch, "Mid-infrared frequency combs," Nat. Photonics **6**(7), 440–449 (2012).
10. J. Haas and B. Mizaikoff, "Advances in Mid-Infrared Spectroscopy for Chemical Analysis," Annu. Rev. Anal. Chem. **9**(1), 45–68 (2016).
11. O. Kara, L. Maidment, T. Gardiner, P. Schunemann, and D. Reid, "Dual-comb spectroscopy in the spectral fingerprint region using OPGaP optical parametric oscillators," Opt. Express **25**(26), 32713–32721 (2017).
12. H. Timmers, A. Kowligy, A. Lind, F. C. Cruz, N. Nader, M. Silfies, G. Ycas, T. K. Allison, P. G. Schunemann, S. B. Papp, and S. A. Diddams, "Molecular fingerprinting with bright, broadband infrared frequency combs," Optica **5**(6), 727 (2018).
13. B. Shan and Z. Chang, "Dramatic extension of the high-order harmonic cutoff by using a long-wavelength driving field," Phys. Rev. A **65**(1), 011804 (2001).
14. H. Liu, Y. Li, Y. S. You, S. Ghimire, T. F. Heinz, and D. A. Reis, "High-harmonic generation from an atomically thin semiconductor," Nat. Phys. **13**(3), 262–265 (2017).

Optics EXPRESS

15. K. Nakagawa, H. Hirori, S. A. Sato, H. Tahara, F. Sekiguchi, G. Yumoto, M. Saruyama, R. Sato, T. Teranishi, and Y. Kanemitsu, "Size-controlled quantum dots reveal the impact of intraband transitions on high-order harmonic generation in solids," Nat. Phys. **18**(8), 874–878 (2022).
16. C. Heide, Y. Kobayashi, D. R. Baykusheva, D. Jain, J. A. Sobota, M. Hashimoto, P. S. Kirchmann, S. Oh, T. F. Heinz, D. A. Reis, and S. Ghimire, "Probing topological phase transitions using high-harmonic generation," Nat. Photonics **16**(9), 620–624 (2022).
17. R. Budriūnas, K. Jurkus, M. Vengris, and A. Varanavičius, "Long seed, short pump: converting Yb-doped laser radiation to multi-μJ few-cycle pulses tunable through 2.5–15 μm," Opt. Express **30**(8), 13009 (2022).
18. M. Bradler, C. Homann, and E. Riedle, "Mid-IR femtosecond pulse generation on the microjoule level up to 5 μm at high repetition rates," Opt. Lett. **36**(21), 4212 (2011).
19. D. Brida, M. Marangoni, C. Manzoni, S. D. Silvestri, and G. Cerullo, "Two-optical-cycle pulses in the mid-infrared from an optical parametric amplifier," Opt. Lett. **33**(24), 2901 (2008).
20. A. A. Lanin, A. A. Voronin, E. A. Stepanov, A. B. Fedotov, and A. M. Zheltikov, "Frequency-tunable sub-two-cycle 60-MW-peak-power free-space waveforms in the mid-infrared," Opt. Lett. **39**(22), 6430 (2014).
21. E. A. Stepanov, A. A. Lanin, A. A. Voronin, A. B. Fedotov, and A. M. Zheltikov, "Solid-State Source of Subcycle Pulses in the Midinfrared," Phys. Rev. Lett. **117**(4), 043901 (2016).
22. D. Sanchez, M. Hemmer, M. Baudisch, S. L. Cousin, K. Zawilski, P. Schunemann, O. Chalus, C. Simon-Boisson, and J. Biegert, "7 μm, ultrafast, sub-millijoule-level mid-infrared optical parametric chirped pulse amplifier pumped at 2 μm," Optica **3**(2), 147 (2016).
23. S. Ashihara and Y. Kawahara, "Spectral broadening of mid-infrared femtosecond pulses in GaAs," Opt. Lett. **34**(24), 3839 (2009).
24. G. Andriukaitis, S. Ališauskas, A. Pugžlys, A. Baltuška, L. Tan, H. J. Lim, P. P. Boon, K. Balskus, and A. Michailovas, "Micro-Joule Octave Spanning Pulses at 6 μm from a Hybrid Femtosecond OPA," in *Lasers, Sources, and Related Photonic Devices* (OSA, 2012), p. AM1A.6.
25. H. Liang, P. Krogen, Z. Wang, H. Park, T. Kroh, K. Zawilski, P. Schunemann, J. Moses, L. F. DiMauro, F. X. Kärtner, and K.-H. Hong, "High-energy mid-infrared sub-cycle pulse synthesis from a parametric amplifier," Nat. Commun. **8**(1), 141 (2017).
26. T. Kanai, P. Malevich, S. S. Kangaparambil, K. Ishida, M. Mizui, K. Yamanouchi, H. Hoogland, R. Holzwarth, A. Pugzlys, and A. Baltuska, "Parametric amplification of 100 fs mid-infrared pulses in ZnGeP_2 driven by a Ho:YAG chirped-pulse amplifier," Opt. Lett. **42**(4), 683 (2017).
27. L. von Grafenstein, M. Bock, D. Ueberschaer, K. Zawilski, P. Schunemann, U. Griebner, and T. Elsaesser, "5 μm few-cycle pulses with multi-gigawatt peak power at a 1 kHz repetition rate," Opt. Lett. **42**(19), 3796 (2017).
28. S. Qu, X. Zou, K. Liu, W. Li, S. H. Luen, Q. J. Wang, Y. Zhang, and H. Liang, "Micro-joule, 10 kHz, sub-two-cycle, long wavelength mid-infrared laser source based on the 9 μm OPCPA," in *Laser Congress 2019 (ASSL, LAC, LS&C)* (OSA, 2019), p. AM2A.6.
29. P. Fuertjes, M. Bock, L. von Grafenstein, D. Ueberschaer, U. Griebner, and T. Elsaesser, "Few-cycle 65-μJ pulses at 11.4 μm for ultrafast nonlinear longwave-infrared spectroscopy," Optica **9**(11), 1303 (2022).
30. B. E. Schmidt, N. Thiré, M. Boivin, A. Laramée, F. Poitras, G. Lebrun, T. Ozaki, H. Ibrahim, and F. Légaré, "Frequency domain optical parametric amplification," Nat. Commun. **5**(1), 3643 (2014).
31. P. Lassonde, F. Legare, B. E. Schmidt, N. Thire, L. Arissian, G. Ernotte, F. Poitras, T. Ozaki, A. Laramee, M. Boivin, and H. Ibrahim, "High Gain Frequency Domain Optical Parametric Amplification," IEEE J. Sel. Top. Quantum Electron. **21**(5), 1–10 (2015).
32. V. Gruson, G. Ernotte, P. Lassonde, A. Laramée, M. R. Bionta, M. Chaker, L. Di Mauro, P. B. Corkum, H. Ibrahim, B. E. Schmidt, and F. Legaré, "2.5 TW, two-cycle IR laser pulses via frequency domain optical parametric amplification," Opt. Express **25**(22), 27706 (2017).
33. B. E. Schmidt, P. Lassonde, G. Ernotte, M. Clerici, R. Morandotti, H. Ibrahim, and F. Légaré, "Decoupling Frequencies, Amplitudes and Phases in Nonlinear Optics," Sci. Rep. **7**(1), 7861 (2017).
34. A. Leblanc, G. Dalla-Barba, P. Lassonde, A. Laramée, B. E. Schmidt, E. Cormier, H. Ibrahim, and F. Légaré, "High-field mid-infrared pulses derived from frequency domain optical parametric amplification," Opt. Lett. **45**(8), 2267 (2020).
35. S. Akturk, X. Gu, P. Gabolde, and R. Trebino, "The general theory of first-order spatio-temporal distortions of Gaussian pulses and beams," Opt. Express **13**(21), 8642–8661 (2005).
36. T. P. Butler, D. Gerz, C. Hofer, J. Xu, C. Gaida, T. Heuermann, M. Gebhardt, L. Vamos, W. Schweinberger, J. A. Gessner, T. Siefke, M. Heusinger, U. Zeitner, A. Apolonski, N. Karpowicz, J. Limpert, F. Krausz, and I. Pupeza, "Watt-scale 50-MHz source of single-cycle waveform-stable pulses in the molecular fingerprint region," Opt. Lett. **44**(7), 1730 (2019).
37. Q. Cao, F. X. Kärtner, and G. Chang, "Towards high power longwave mid-IR frequency combs: power scalability of high repetition-rate difference-frequency generation," Opt. Express **28**(2), 1369 (2020).
38. A. Andrianov, A. Szabo, A. Sergeev, A. Kim, V. Chvykov, and M. Kalashnikov, "Computationally efficient method for Fourier transform of highly chirped pulses for laser and parametric amplifier modeling," Opt. Express **24**(23), 25974–25982 (2016).
39. Sz. Toth, "Optimization of high peak power few-cycle optical parametric chirped pulse amplifier systems," Doctoral dissertation, University of Szeged (2021).

Optics EXPRESS

40. K. Liu, H. Liang, W. Li, X. Zou, S. Qu, T. Lang, Y. Zhang, and Q. J. Wang, "Microjoule Sub-Two-Cycle Mid-Infrared Intrapulse-DFG Driven by 3-μm OPCPA," IEEE Photonics Technol. Lett. **31**(21), 1741–1744 (2019).
41. K. Liu, H. Liang, L. Wang, S. Qu, T. Lang, H. Li, Q. J. Wang, and Y. Zhang, "Multimicrojoule GaSe-based midinfrared optical parametric amplifier with an ultrabroad idler spectrum covering 4.2–16 μm," Opt. Lett. **44**(4), 1003 (2019).
42. A. Leblanc, P. Lassonde, S. Petit, J.-C. Delagnes, E. Haddad, G. Ernotte, M. R. Bionta, V. Gruson, B. E. Schmidt, H. Ibrahim, E. Cormier, and F. Légaré, "Phase-matching-free pulse retrieval based on transient absorption in solids," Opt. Express **27**(20), 28998 (2019).
43. G. Cerullo and S. De Silvestri, "Ultrafast optical parametric amplifiers," Rev. Sci. Instrum. **74**(1), 1–18 (2003).
44. A. Leblanc, P. Lassonde, G. Dalla-Barba, E. Cormier, H. Ibrahim, and F. Légaré, "Characterizing the carrier-envelope phase stability of mid-infrared laser pulses by high harmonic generation in solids," Opt. Express **28**(12), 17161 (2020).